ARTICLE

Transparent Organic P-Dopant in Carbon Nanotubes: Bis(trifluoromethanesulfonyl)imide

Soo Min Kim,[†] Young Woo Jo,[†] Ki Kang Kim,[‡] Dinh Loc Duong,[†] Hyeon-Jin Shin,[§] Jong Hun Han,[#] Jae-Young Choi,[§] Jing Kong,*[,‡] and Young Hee Lee*[,†]

[†]BK21 Physics Division, Department of Energy Science, and Center for Nanotubes and Nanostructured Composites, Sungkyunkwan Advanced Institute of Nanotechnology, Sungkyunkwan University (SKKU), Suwon 440-746, Korea, [‡]Department of Electrical Engineering and Computer Sciences, Massachusetts Institute of Technology (MIT), Cambridge, Massachusetts 02139, United States, [§]Display Lab, Samsung Advanced Institute of Technology (SAIT), P.O. Box 111, Suwon 440-600, Korea, and [#]Nanomaterials-Processing Group/Energy/Nano Materials Research Center Korea Electronics Technology Institute (KETI) 68 Yatap-dong, Bundang-gu, Seongnam-si, Gyeonggi-do 463-816, Korea

ABSTRACT We propose bis(trifluoromethanesulfonyl)imide $[(CF_3SO_2)_2N]^-$ (TFSI) as a transparent strong electron-withdrawing p-type dopant in carbon nanotubes (CNTs). The conventional p-dopant, $AuCl_3$, has several drawbacks, such as hygroscopic effect, formation of Au clusters, decrease in transmittance, and high cost in spite of the significant increase in conductivity. TFSI is converted from bis(trifluoromethanesulfonyl)amine (TFSA) by accepting electrons from CNTs, subsequently losing a proton as a characteristic of a Brønsted acid, and has an inductive effect from atoms with high electronegativity, such as halogen, oxygen, and nitrogen. TFSI produced a similar improvement in conductivity to $AuCl_3$, while maintaining high thermal stability, and no appreciable change in transmittance with no cluster formation. The effectiveness of TFSI was compared with that of other derivatives.

KEYWORDS: carbon nanotube · doping · stability · sheet resistance · transmittance · conductivity

Single-walled carbon nanotubes (SWCNTs) have potential applications in soft electronic devices owing to their unique electronic and mechanical properties.[1−4] Nevertheless, various issues, such as separation of either metallic or semiconducting SWCNTs and control of doping and metal-CNT contact, are still an impediment to real applications.[5−7] A series of n-type and p-type dopants for CNTs have been developed.[8−11] Alkali metals oxidize easily under ambient conditions despite their excellent electron-donating ability.[12] Poly(ethyleneimine) is a good n-type dopant due to the presence of an electron-donating amine group.[13] Nevertheless, it is easily oxidized again in air, and provides a large leakage current, thereby reducing the on/off ratio in transistors.[9,13] Recently, environmentally stable viologen derivatives and β-nicotinamide adenine dinucleotide-reduced dipotassium salt were used for n-type doping in CNT transistors.[8,9] These derivatives showed a high on/off ratio and good environmental stability for up to a few months. Although p-type dopants are relatively stable under ambient conditions due to their oxidation potentials, some still show environmental evolution. Simple approaches using acid solution reduce the sheet resistance by removing unnecessary surfactants and could also damage PET substrate to make it hazy. The environmental stability also has been an issue.[14] So far, $AuCl_3$ shows the best performance as a p-type dopant owing to its high redox potential.[11] The sheet resistance of CNT films has been decreased up to 90%.[11] However, $AuCl_3$ has several drawbacks preventing its applications to electronic devices, such as transistors and flexible conducting films. These include the high hygroscopic effect that degrades the environmental stability under ambient conditions, formation of Au clusters on the CNT surface and the degradation of transmittance and Au ions involve the generation of impurity levels due to strong chemisorptions to the CNT surface.[15,16] Moreover, $AuCl_3$ is expensive and is not a good choice for industrial applications. Therefore, another alternative material without such drawbacks is desirable.

The choice of materials is limited due to the required conditions of the dopant, such as effective electron-withdrawing ability with environmental stability, maintaining high transmittance without agglomeration, and low cost. Organic complex dopants are normally inexpensive but environmentally unstable. However, bis(trifluoromethanesulfonyl)imide $[(CF_3SO_2)_2N]^-$ (TFSI) is a strong electron-withdrawing group (EWG) with environmental stability owing to its hydrophobicity, strong bonding character,

*Address correspondence to jingkong@mit.edu, leeyoung@skku.edu.

Received for review August 27, 2010 and accepted September 28, 2010.

Published online October 14, 2010. 10.1021/nn102175h

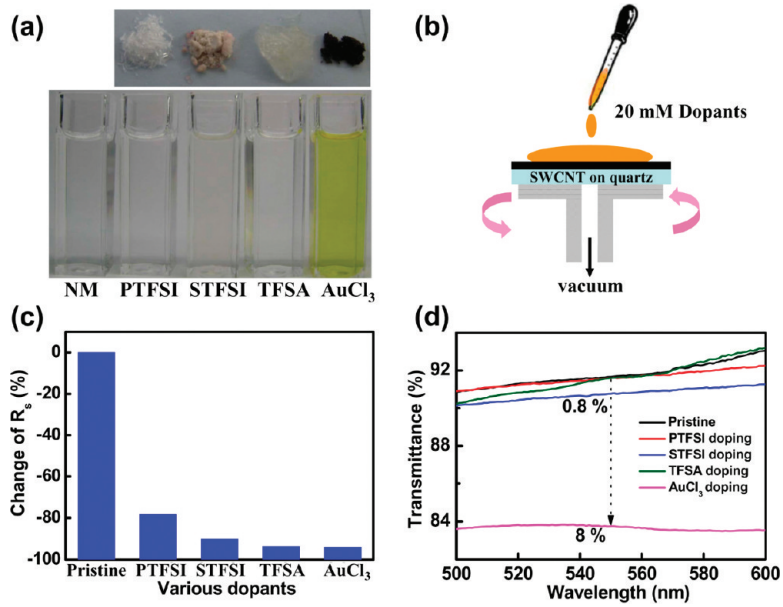

Figure 1. (a) Color of the chosen powders: PTFSI, STFSI, TFSA, $AuCl_3$ from the left. The bottom panel shows the respective solution dissolved in nitromethane (NM). (b) Schematic of spin-casting doping, (c) The change in sheet resistance after doping. (d) The transmittance for the pristine CNT and PTFSI-doped, STFSI-doped, TFSA-doped, and $AuCl_3$-doped CNT on quartz substrate.

and high transmittance.[17] TFSI contains high electronegativity atoms, such as fluoro, sulfur, oxygen, and nitrogen, which induces local charge from adjacent materials, known as an inductive effect.[18]

In this study, a series of TFSI with different acid derivatives were selected to examine their different doping ability on CNTs and compare the change of CNT film in transmittance. The prepared dopant solution in nitromethane was spin-casted onto a random network SWCNTs film. The sheet resistance after doping particularly with TFSI decreased significantly to a similar level to $AuCl_3$ and showed a negligible change in transmittance while maintaining its environmental and thermal stability.

RESULTS AND DISCUSSION

The effectiveness of TFSI doping was compared with that of the other acid derivatives. Three derivatives with TFSI functional groups and $AuCl_3$ were used for comparison. Figure 1a shows the color of the chosen powders (PTFSI, STFSI, TFSA, and $AuCl_3$ from the left, see Table 1 for notation). The PTFSI and TFSA powders were colorless, whereas STFSI and $AuCl_3$ have a brown and dark red color, respectively, due to the presence of gold and silver. When dissolved in nitromethane, a distinct yellow color was revealed in the $AuCl_3$ solution and the STFSI solution became slightly opaque due to the ions of metals. The dopant solution was simply spin-casted on the prepared SWCNTs film (Figure 1b). The sheet resistance of the SWCNT films was measured after doping to estimate the doping ability of each dopant. The sheet resistance of TFSA after doping was reduced by 93.6% compared to the pristine sample (600 Ω/sq at 85% transmittance), which is similar to 94.2% for $AuCl_3$ doping. The other types of

TABLE 1. Material Parameters of the Various Dopants: Nomenclature, Structure, Melting Point, and Price

Entry	Nomenclature	Structure	M.P.	Price (USD/1g)
PTFSI	N-phenyl-bis(trifluoromethane sulfonyl)imide	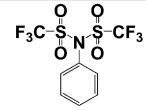	100~102 ℃	10.6
STFSI	Silver bis(trifluoromethane sulfonyl)imide	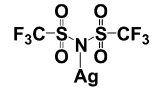	248.8 ℃	100.2
TFSA	Bis(trifluoromethanesulfonyl) amine	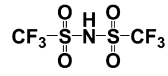	46~57 ℃	20.0
$AuCl_3$	Gold (III) chloride	$AuCl_3$	45~47 ℃	139.0

TABLE 2. The Total Change in Sheet Resistance Relative to the Original Value after 80 Days (%)

chemical	PTFSI	STFSI	TFSA	$AuCl_3$
before annealing	−78.1	−90.0	−93.6	−94.2
after annealing	−70.9	−87.7	−92.2	−92.9
difference	−7.2	−2.3	−1.4	−1.3

TFSI showed a relatively small decrease in sheet resistance compared to TFSA, as shown in Figure 1c and Table 2. The reason why they showed different levels of reduction will be discussed later. Since TFSI has no optical absorption in the visible range, the decrease in transmittance in the case of TFSA doping was negligible compared to that of the pristine sample over a wide range of spectra, as shown in Figure 1d.[20] In contrast, the STFSI-doped and $AuCl_3$-doped sample showed significant degradation in transmittance (0.8% and 8% at 550 nm) (Figure 1d) due to the existence of Ag and Au clusters formed during doping. To clarify the change in transmittance, the samples were observed by SEM. The most intriguing feature of TFSI doping compared to $AuCl_3$ is the disappearance of metal clusters. As illustrated in Figure 2a−e, STFSI forms Ag particles after reduction, similar to $AuCl_3$ doping. On the other hand, TFSA and PTFSI did not show such particles. The formation of metal particles affects the level of their light absorption and scattering significantly. The decrease in transmittance in the case of TFSA doping was negligible compared to that of the pristine sample over a wide range of spectra, as shown in Figure 1d. This is certainly advantageous for TFSA compared to its counterpart $AuCl_3$ for applications to transparent conducting films.

The environmental and thermal stability of CNT film after doping is one of the important issues for commercial application. The doped CNT film was further annealed at 150 °C in air to test the thermal stability, followed by exposure under ambient conditions for 80 days to test the environmental stability. Figure 3a shows the environmental stability of the doped sample left for up to 80 days. The sheet resistance increased slightly with time regardless of the dopant type. In particular, high stability was maintained for the $AuCl_3$ and TFSA cases. The TFSI anions were solvated with the respective cations in solution. TFSI has strong electron-withdrawing power and can easily extract electrons from the adjacent SWCNTs, and is stabilized by accepting electrons from the CNTs. The binding energy of TFSI relies on the type of cation, which will be discussed later. After annealing, the sheet resistance of the annealed sample (Figure 3b) increased initially but maintained high stability after 6 h with the exception of PTFSI. Although TFSI was stable with an annealing at 150 °C, some of the TFSI functional groups were detached during annealing, as discussed later. The sheet resistance was increased further, albeit slightly, by leaving the samples under ambient conditions for 80 days.

The doping effect was also clearly shown in the G-band of the Raman spectra (Figure 4a,b).[21] At an excitation energy of 1.96 eV, the metallic SWCNTs (E_{11}^{M}) were mostly excited in the pristine sample, as demonstrated by the presence of a large Breit−Wigner−Fano (BWF) line at the lower energy side of the G-band near 1590 cm^{-1} in Figure 4a.[22] The peak positions of the G^+-band of the dopants were upshifted. This change is con-

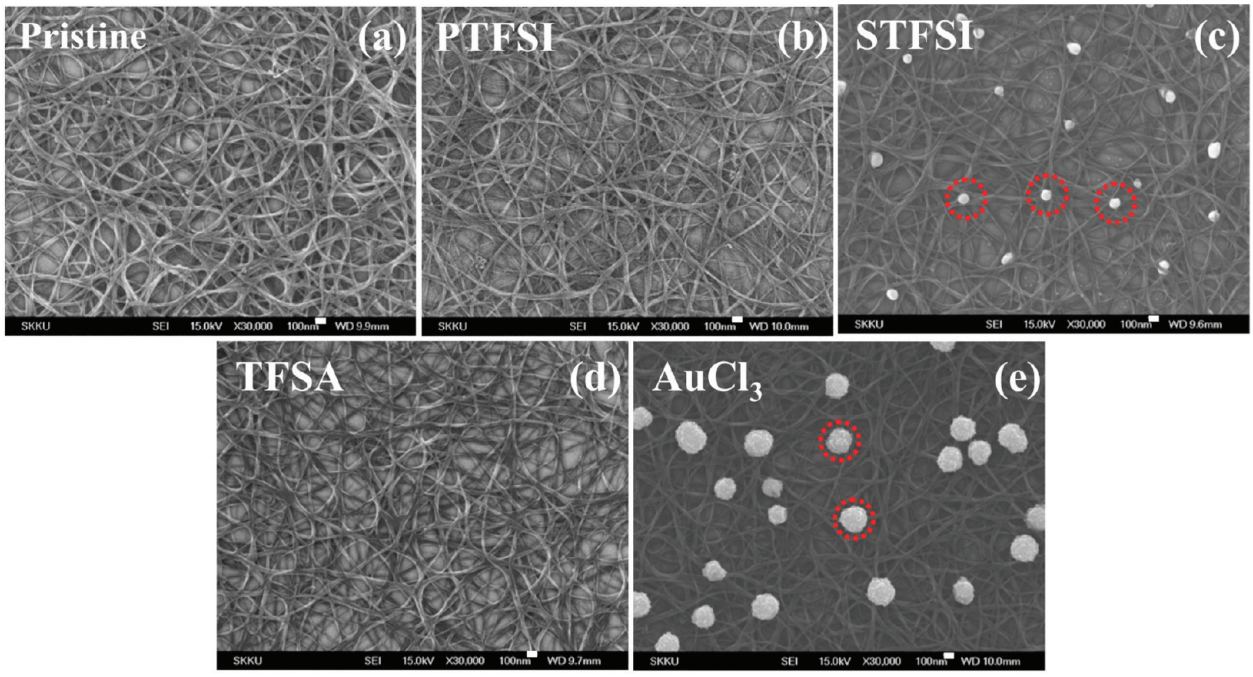

Figure 2. FE-SEM images of the films for (a) pristine, (b) PTFSI, (c) STFSI, (d) TFSA, and (e) $AuCl_3$ doped (20 mM) samples in nitromethane. The surface morphology of PTFSI and TFSA except for STFSI and $AuCl_3$ remained clean after doping similar to the pristine sample. However, in the case of STFSI and $AuCl_3$ doping, the Ag and Au particles were clearly seen in red open circles.

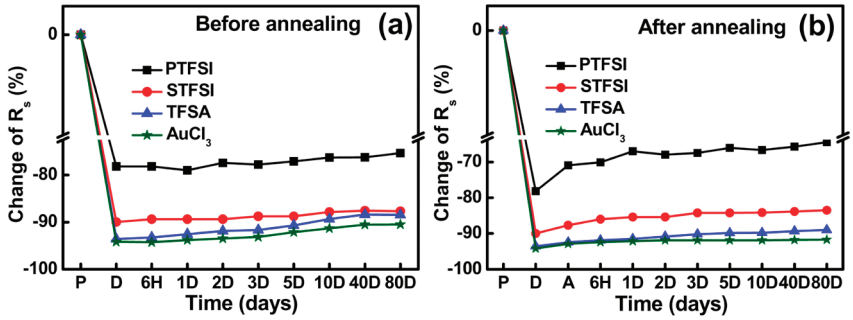

Figure 3. The change of sheet resistance value after doping, followed by thermal annealing at 150 °C for 1 h in air, and then after 80 days under ambient conditions. Aging of the sample with time (a) under ambient conditions and (b) after thermal annealing conditions. P: pristine, D: doped, A: annealed, 6H: 6 h, and *n*D: *n* days.

sistent with the previous report of the phonon stiffening effect by p-type doping.[11,23] To analyze the doping effect on the metallic tube, The G-band was deconvoluted into 6 peaks: two metallic and four semiconducting tubes.[19] As a consequence of electron transfer from the CNT to dopant, the BWF component was also reduced in a similar manner to $AuCl_3$, particularly in the case of TFSA.[19,22] This increases the hole carrier concentration in the CNTs, which increases the conductivity or decreases the sheet resistance. Similar behavior was also observed in the samples after annealing, as shown in Figure 4b. The results are summarized in Figure 4c. No significant change in the integrated metallic area of the G-band after annealing was observed in the case of STFSI, TFSA, and $AuCl_3$, as shown in the histogram of Figure 4c. Interestingly, there is a strong correlation between the BWF component and the peak shift of the G′-band.[24] This trend is in line with the trend of the sheet resistance shown in Figure 1c. Despite the same TFSI group that is shared in all acid derivatives, the amount of charge transfer observed in the Raman spectra, and as a consequence the change in sheet resistance, vary with the type of cationic part. TFSA with a −NH group easily loses proton and transforms to TFSI during electron acceptance from the adjacent CNT, which is a characteristic of a Brønsted acid.[25,26] In the case of STFSI with −NAg, silver ions are detached during CNT adsorption similar to TFSA. These silver ions react further with other CNTs (or different local sites of CNTs) and are partially reduced to silver particles (see Figure 2). To confirm this, atomic composition of Ag atoms in STFSI was determined by fitting core level spectra of each atom. After doping, about 90% of STFSI was reduced to Ag atoms but about 10% of STFSI still remained unreduced (see the Supporting Information, Figure S1). Therefore, the interaction of CNTs with TFSI becomes weaker due to the steric hindrance from AgN-CNT bonding and the amount of

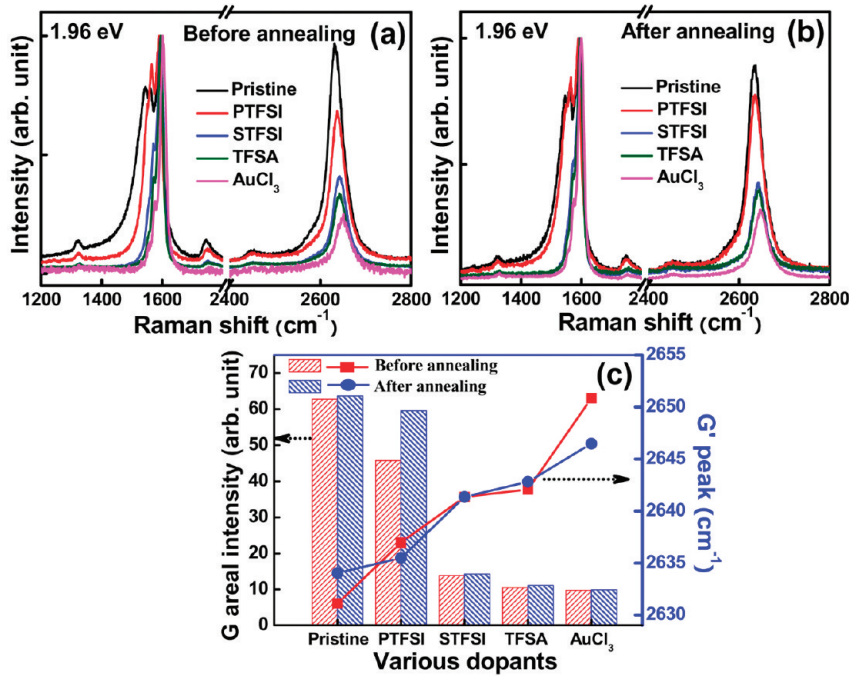

Figure 4. Raman spectra of the doped SWCNTs after 80 days (a) before annealing and (b) after annealing. (c) Relationship between the metallic areal intensity of the G band and the G′ band peak position. A laser with an excitation energy of 1.96 eV was used.

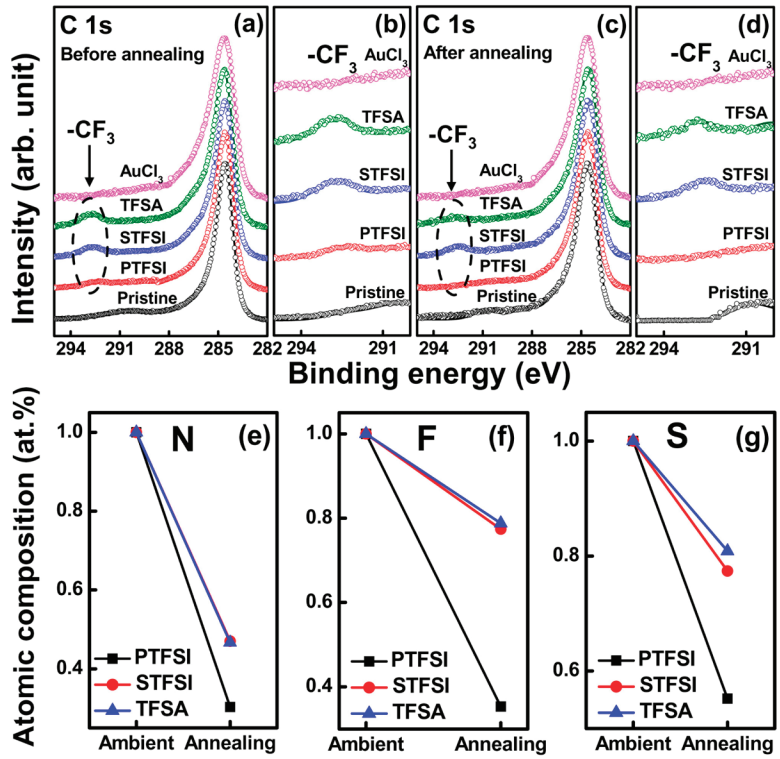

Figure 5. XPS spectra of $-CF_3$ peak (a, b) after doping and (c, d) after thermal annealing at 150 °C for 1 h in air. Change in the chemical composition plot after doping and after annealing for (e) nitrogen, (f) fluoro, and (g) sulfur atom.

electron transfer from CNTs to TFSI is reduced. This increases the sheet resistance of STFSI film slightly compared to that of the TFSA films.

The change in sheet resistance with dopant can be explained in general by an analysis of the XPS data. Charge transfer during adsorption of TFSI by CNT could be monitored by nitrogen, fluoro, and sulfur in the TFSI group. For example, the doping effect, which can be represented by the N1s, F1s, and S2p peak shift, was well observed in the case of STFSI (see the Supporting Information, Figure S2).[27,28] However, XPS of the other TFSI derivatives was not possible due to the low melting temperatures, as indicated in Table 1. C1s peak shift in general indicates the Fermi level shift induced by charge transfer.[27] However, in this case, the CNTs and dopants contained carbon atoms, making it ambiguous in interpretation, as shown in Figure 5a. Instead, the peak related to CF_3 was observed near 292 eV (Figure 5b).[28] The peak intensity was highest in TFSA and lowest in PTFSI, which again reflects the change in sheet resistance in Figure 1c. After annealing, these peaks still remained, even though the intensities of CF_3 were reduced consistently, as shown in Figure 5c,d. Since the TFSI group contains nitrogen, fluoro, and sulfur atoms, these XPS peaks before and after annealing were obtained and normalized to those before annealing, and are plotted in Figure 5e−g. Although STFSI and TFSI showed a similar decrease in atomic percentage after annealing, PTFSI showed a larger decrease than the others, revealing similar behavior for all atoms. This suggests that PTFSI is detached more easily during annealing than the other types. In other words, the binding energy of PTFSI on a CNT surface is weaker than that of the others, whereas the binding energies of STFSI and TFSA are similar.

The role of cations was confirmed in the FTIR spectra. In the case of PTFSI-doped CNT, the phenyl group peaks near 1400 (H bending) and 3000 cm^{-1} (H stretching) disappeared after doping (Figure 6a). Phenyl groups interact by $\pi-\pi$ stacking with the CNT surface, which suppresses the related peaks.[29] This weakens the TFSI interaction with the CNT surface due to the steric hindrance from phenyl−CNT bonding. As a consequence, PTFSI detaches easily from the CNT surface during annealing and has thus less doping ability, in agreement with the doping ability shown in the previous discussion. The peaks were broadened and shifted after doping compared to the distinct powder peaks, regardless of the dopants (Figure 6). This indicates complicated charge transfer from the CNTs to the TFSI group. In the case of the STFSI-doped CNT film, the AgN peak near 1600 cm^{-1} disappeared after doping, indicating the solvation of Ag ions. XPS revealed new bonding peaks of C−N near 399 eV and C−N^+ near 401 eV, as shown in the inset of Figure 6c.[30,31] The −NH peak near 3400 cm^{-1} in the case of TFSA disappeared after doping, as expected from Brønsted acidic reaction, again revealing similar C−N binding character to the STFSI case. The doping ability of STFSI is slightly lower than that of TFSA. It might originate from relatively less

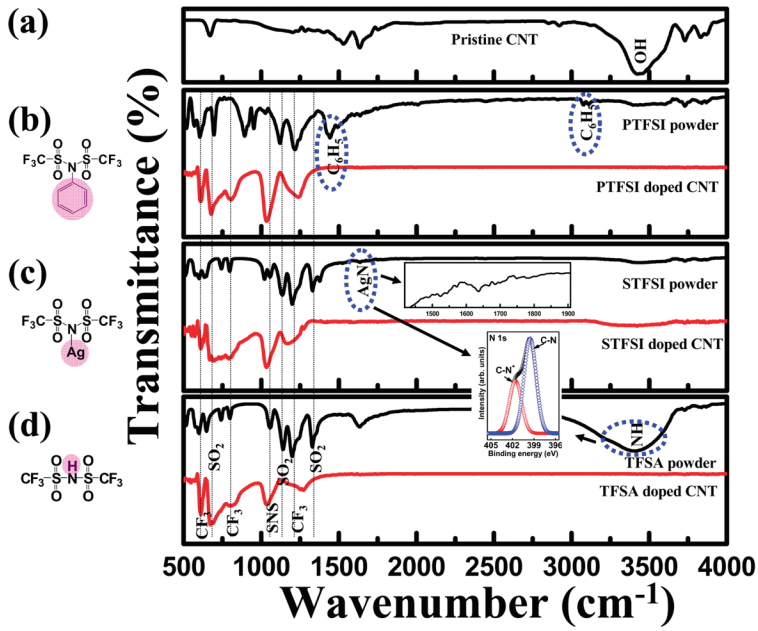

Figure 6. FTIR spectra of (a) pristine CNT powder, (b) PTFSI powder, PTFSI-doped CNT film, (c) STFSI powder, STFSI-doped CNT film, and (d) TFSA powder, TFSA-doped CNT film. The SO_2, CF_3, and SNS peaks are marked in the dotted lines.

reaction of solvated Ag with CNT, compared to the complete Brønsted acidic reaction in the case of TFSA.

CONCLUSION

This study evaluated the feasibility of a new transparent organic p-type dopant for carbon nanotubes, which was thermally and environmentally stable without degrading the transmittance with doping, while maintaining similar doping ability to $AuCl_3$. Among the acidic derivatives of TFSI, TFSA was found to be the best in terms of the binding energy and charge transfer. In particular, TFSA showed no degradation in transmittance while maintaining a similar improvement in the sheet resistance to the $AuCl_3$ case. Therefore, this dopant can be used in future CNT devices, such as transparent conducting films and the thin film transistor.

EXPERIMENTAL SECTION

Film Preparation. Purified arc-discharge SWCNTs (Iljin Nanotech Co., Ltd., purity: 93%) with a mean diameter of 1.5 nm (range, 1.2 to 1.8 nm) and a typical length of a few micrometers were used in this experiment. The SWCNTs (2 mg) were added to 30 mL of 1,2-dichloroethane (DCE: anhydrous, 99.8% Sigma-Aldrich) followed by sonication in a bath type sonicator (RK 106, Bandelin Electronic, Berlin, Germany) for 6 h. The solution was centrifuged (Hanil Science Industrial Co., Ltd., Mega 17R) at 8000 rpm for 10 min. The supernatant of the resulting solution was sprayed on a quartz substrate (2×2 cm^2) with an Ar gas brush pistol (Gunpiece GP-1, Fuso Seiki Co., Ltd.) and further heat-treated to 900 °C for 1 h under an Ar atmosphere to exclude solvent effect.[19] This sample was assigned as the pristine sample.

Doping and Annealing Procedure. Several doping materials were chosen: *N*-phenylbis(trifluoromethanesulfonyl)imide ($C_6H_5N(SO_2CF_3)_2$: purity 99%, Sigma-Aldrich), silver bis(trifluoromethanesulfonyl)imide ($AgN(SO_2CF_3)_2$: purity 97%, Sigma-Aldrich), bis(trifluoromethanesulfonyl)amine ($HN(CF_3SO_2)_2$: purity 95%, Sigma-Aldrich), and gold chloride ($AuCl_3$: purity 99%, Sigma-Aldrich) powder, as listed in Table 1. The basic anion unit of organic molecules is the bis(trifluoromethanesulfonyl)imide functional group (TFSI) with various cationic parts. These were dissolved in nitromethane (Sigma-Aldrich) to a concentration of 20 mM. One 400 μL drop of the doping solution was placed onto the SWCNT film. After a residual time of 30 s, the solvent was spin-coated at 2500 rpm for 1 min (Midas System, Spin 2000). The film was exposed to ambient conditions for several hours before the measurements. To examine the thermal stability of CNT film, the CNT film after doping was annealed at 150 °C for 1 h in air. The sheet resistance of CNT film was evaluated up to 80 days to evaluate the stability of CNT film under ambient condition.

Measurement. The sheet resistance was measured at room temperature with a four-point method (Keithley 2000 multimeter). Raman spectroscopy (Renishaw, RM-1000 Invia) with an excitation energy of 1.96 eV (632.8 nm, He−Ne laser) was used to characterize the optical properties of doped SWCNTs. X-ray photoelectron spectroscopy (XPS, ESCA2000, VG Microtech, England) was carried out to check for the presence of residual material and the degree of doping. The surface morphology of the film was observed by FE-SEM (JSM700F, JEOL) at 10 keV while simultaneous compositional analysis was obtained in energy-dispersive X-ray spectroscopy (EDX) mode. To elucidate the functional group on CNT after doping, CNT film and dopants were characterized by Fourier-transform infrared spectroscopy (FTIR spectroscopy, Bruker IFS-66/S). The FTIR samples of several doping materials were in the form of a powder that was ground with KBr to make a pellet.

Acknowledgement This study was supported by the STAR-faculty program and WCU (World Class University) program through the KRF funded by the MEST (R31-2008-000-10029-0), the Industrial Technology Development Program (10031734) of the Ministry of Knowledge Economy (MKE), and the IRDP of NRF

(2010-00429) through a grant provided by MEST in 2010 in Korea. S.M.K. acknowledges a Seoul Science Fellowship.

Supporting Information Available: Ag 3d core level spectra of STFSI-CNT (Figure S1) and XPS spectra of STFSI-CNT sample (Figure S2). This material is available free of charge *via* the Internet at http://pubs.acs.org.

REFERENCES AND NOTES

1. Geng, H.-Z.; Kim, K. K.; So, K. P.; Lee, Y. S.; Chang, Y.; Lee, Y. H. Effect of Acid Treatment on Carbon Nanotube-Based Flexible Transparent Conducting Films. *J. Am. Chem. Soc.* **2007**, *129*, 7758–7759.
2. An, K. H.; Lee, Y. H. Electronic-Structure Engineering of Carbon Nanotubes. *NANO* **2006**, *1*, 115–138.
3. Saito, R.; Fujita, M.; Dresselhaus, G.; Dresselhaus, M. S. Electronic Structure of Chiral Graphene Tubules. *Appl. Phys. Lett.* **1992**, *60*, 2204–2206.
4. Yu, M.-F.; Files, B. S.; Arepalli, S.; Ruoff, R. S. Tensile Loading of Ropes of Singlewall Carbon Nanotubes and their Mechanical Properties. *Phys. Rev. Lett.* **2000**, *84*, 5552–5555.
5. Arnold, M. S.; Green, A. A.; Hulvat, J. F.; Stupp, S. I.; Hersam, M. C. Sorting Carbon Nanotubes by Electronic Structure using Density Differentiation. *Nat. Nanotechnol.* **2006**, *1*, 60–65.
6. Kim, K. K.; Yoon, S.-M.; Park, H. K.; Shin, H.-J.; Kim, S. M.; Bae, J. J.; Cui, Y.; Kim, J. M.; Choi, J.-Y.; Lee, Y. H. Doping Strategy of Carbon Nanotubes with Redox Chemistry. *New J. Chem.*, **2010**, *34*, 2183−2188.
7. Lim, S. C.; Jang, J. H.; Bae, D. J.; Han, G. H.; Lee, S.; Yeo, I.; Lee, Y. L. Contact Resistance between Metal and Carbon Nanotube Interconnects: Effect of Work Function and Wettability. *Appl. Phys. Lett.* **2009**, *95*, 264103/1–3.
8. Kim, S. M.; Jang, J. H.; Kim, K. K.; Park, H. K.; Bae, J. J.; Yu, W. J.; Lee, I. H.; Kim, G.; Duong, D. L.; Kim, U. J.; et al. Reduction-Controlled Viologen in Bisolvent as an Environmentally Stable n-Type Dopant for Carbon Nanotubes. *J. Am. Chem. Soc.* **2009**, *131*, 327–331.
9. Kang, B. R.; Yu, W. J.; Kim, K. K.; Park, H. K.; Kim, S. M.; Park, Y.; Kim, G.; Shin, H.-J.; Kim, U. J.; Lee, E.-H.; et al. Restorable Type Conversion of Carbon Nanotube Transistor Using Pyrolytically Controlled Antioxidizing Photosynthesis Coenzyme. *Adv. Funct. Mater.* **2009**, *19*, 2553–2559.
10. Yoon, S.-M.; Kim, S. J.; Shin, H.-J.; Benayad, A.; Choi, S. J.; Kim, K. K.; Kim, S. M.; Park, Y. J.; Kim, G.; Choi, J.-Y.; et al. Selective Oxidation on Metallic Carbon Nanotubes by Halogen Oxoanions. *J. Am. Chem. Soc.* **2008**, *130*, 2610–2616.
11. Kim, K. K; Bae, J. J.; Park, H. K.; Kim, S. M.; Geng, H.-Z.; Park, K. A.; Shin, H.-J.; Yoon, S.-M.; Benayad, A.; Choi, J.-Y.; et al. Fermi Level Engineering of Single-Walled Carbon Nanotubes by $AuCl_3$ Doping. *J. Am. Chem. Soc.* **2008**, *130*, 12757–12761.
12. Zhou, C.; Kong, J.; Yenilmez, E.; Dai, H. Modulated Chemical Doping of Individual Carbon Nanotubes. *Science* **2000**, *290*, 1552–1555.
13. Shim, M.; Javey, A.; Kam, N. W. S.; Dai, H. Polymer Functionalization for Air-Stable n-Type Carbon Nanotube Field-Effect Transistors. *J. Am. Chem. Soc.* **2001**, *123*, 11512–11513.
14. Chandra, B.; Afzali, A.; Khare, N.; El-Ashry, M. M.; Tulevski, G. S. Stable Charge-Transfer Doping of Transparent Single-Walled Carbon Nanotube Films. *Chem. Mater.* **2010**, *22*, 5179−5183.
15. Lee, I. H.; Kim, U. J.; Son, H. B.; Yoon, S.-M.; Yao, F.; Yu, W. J.; Duong, D. L.; Choi, J.-Y.; Kim, J. M.; Lee, E. H.; et al. Hygroscopic Effects on $AuCl_3$-Doped Carbon Nanotubes. *J. Phys. Chem. B* **2010**, *114*, 11618–11622.
16. Duong, D. L.; Lee, I. H.; Kim, K. K.; Kong, J.; Lee, S. M.; Lee, Y. H. Carbon Nanotube Doping Mechanism in a Salt Solution and Hygroscopic Effect: Density Functional Theory. *ACS Nano*, **2010**, *4*, 5430−5436.
17. Ciprelli, J.-L; Clarisse, C.; Delabouglise, D. Enhanced Stability of Conducting Poly(3-octylthiophene) Thin Films using Organic Nitrosyl Compounds. *Synth. Met.* **1995**, *74*, 217–222.
18. Ong, S. P.; Ceder, G. Investigation of the Effect of Functional Group Substitutions on the Gas-Phase Electron Affinities and Ionization Energies of Room-Temperature Ionic Liquids Ions using Density Functional Theory. *Electrochim. Acta* **2010**, *55*, 3804–3811.
19. Shin, H.-J.; Kim, S. M.; Yoon, S.-M.; Benayad, A.; Kim, K. K.; Kim, S. J.; Park, H. K.; Choi, J.-Y.; Lee, Y. H. Tailoring Electronic Structures of Carbon Nanotubes by Solvent with Electron-Donating and -Withdrawing Groups. *J. Am. Chem. Soc.* **2008**, *130*, 2062–2066.
20. Brissot, C.; Rosso, M.; Chazalviel, J.-N.; Lascaud, S. Concentration Measurements in Lithium/Polymer-Electrolyte/Lithium Cells during Cycling. *J. Power Sources* **2001**, *94*, 212–218.
21. Dresselhaus, M. S.; Dresselhaus, G.; Saito, R.; Jorio, A. Raman Spectroscopy of Carbon Nanotubes. *Phys. Rep.* **2005**, *409*, 47–99.
22. Brown, S. D. M.; Jorio, A.; Corio, P.; Dresselhaus, M. S.; Dresselhaous, G.; Saito, R.; Kneipp, K. Origin of the Breit-Wigner-Fano Lineshape of the Tangential G-band Feature of Metallic Carbon Nanotubes. *Phys. Rev. B* **2001**, *63*, 155414/1–8.
23. Rao, A. M.; Eklund, P. C.; Bandow, S.; Thess, A.; Smalley, R. E. Evidence for Charge Transfer in Doped Carbon Nanotube Bundles from Raman Scattering. *Nature* **1997**, *388*, 257–259.
24. Kim, K. K.; Park, J. S.; Kim, S. J.; Geng, H. Z.; An, K. H.; Yang, C.-M.; Sato, K.; Saito, R.; Lee, Y. H. Dependence of Raman Spectra G′ band Intensity on Metallicity of Single-Wall Carbon Nanotubes. *Phys. Rev. B* **2007**, *76*, 205426/1–8.
25. Yang, Z.; Coutinho, D.; Feng, F.; Ferraris, J. P.; Balkus, K., Jr. Novel Inorganic/Organic Hybrid Electrolyte Membranes. *Prepr. Pap. - Am. Chem. Soc., Div. Fuel Chem.* **2004**, *49*, 599–600.
26. Susan, M. A. B. H.; Noda, A.; Mitsushima, S.; Watanabe, M. Brønsted Acid-Base Ionic Liquids and their use as New Materials for Anhydrous Proton Conductors. *Chem. Commun.* **2003**, 938–939.
27. Geng, H.-Z.; Kim, K. K.; Song, C.; Xuyen, N. T.; Kim, S. M.; Park, K. A.; Lee, D. S.; An, K. H.; Lee, Y. S.; Chang, Y.; et al. Doping and De-Doping of Carbon Nanotube Transparent Conducting Films by Dispersant and Chemical Treatment. *J. Mater. Chem.* **2008**, *18*, 1261–1266.
28. Dedryvere, R.; Leroy, S.; Martinez, H.; Blanchard, F.; Lemordant, D.; Gonbeau, D. XPS Valence Characterization of Lithium Salts as a Tool to Study Electrode/Electrolyte Interfaces of Li-Ion Batteries. *J. Phys. Chem. B* **2006**, *110*, 12986–12992.
29. Yang, Z.; Chen, X.; Chen, C.; Li, W.; Zhang, H.; Xu, L.; Yi, B. Noncovalent-Wrapped Sidewall Functionalization of Multiwalled Carbon Nanotubes with Polyimide. *Polym. Compos.* **2007**, 36–41.
30. Alexander, M. R.; Jones, F. R. Effect of Electrolytic Oxidation upon the Surface Chemistry of type a Carbon Fibres: III. Chemical State, Source and Location of Surface Nitrogen. *Carbon* **1996**, *34*, 1093–1102.
31. Delpeux, S.; Beguin, F.; Benoit, R.; Erre, R.; Manolova, N.; Rashkov, I. Fullerene Core Star-like Polymers-1. Preparation from Fullerenes and Monoazidopolyethers. *Eur. Polym. J.* **1998**, *34*, 905–915.